

# Error bounded compression for weather and climate applications

Langwen Huang<sup>1</sup>, Luigi Fusco<sup>1, 4</sup>, Florian Scheidl<sup>1</sup>, Jan Zibell<sup>2</sup>, Michael Armand Sprenger<sup>2</sup>, Sebastian Schemm<sup>3</sup>, and Torsten Hoefler<sup>1</sup>

This manuscript was compiled on February 26, 2026

As the resolution of weather and climate simulations increases, the amount of data produced is growing rapidly from hundreds of terabytes to tens of petabytes. The huge size becomes a limiting factor for broader adoption, and its fast growth rate will soon exhaust all available storage devices. To address these issues, we present EBCC (Error Bounded Climate-data Compressor). It follows a two-layer compression approach: a base compression layer using JPEG2000 to capture the bulk of the data with a high compression ratio, and a residual compression layer using wavelet transform and SPIHT (Set Partitioning In Hierarchical Trees) encoding to efficiently eliminate long-tail extreme errors. We evaluate EBCC alongside other established compression methods on several benchmarks related to weather and climate science. The benchmarks include error statistics, a case study on primitive and derived variables near a tropical cyclone, evaluation of the closure of the global energy budget, and a Lagrangian air parcel trajectory simulation. EBCC outperforms other methods in the benchmarks at relative error targets ranging from 0.1% to 10% and achieves compression ratios from 15× to more than 300×, respectively. In the energy budget closure and Lagrangian trajectory benchmarks, it can achieve more than 100× compression while keeping errors within the natural variability derived from ERA5 uncertainty members. This verifies the effectiveness of EBCC in creating heavily compressed weather and climate datasets suitable for downstream applications.

Data Compression | Extreme Weather | Benchmark

Numerical weather and climate simulations produce a huge amount of data ranging from hundreds of terabytes to tens of petabytes (1–3). Analyzing these data requires significant storage and computing resources, which are only available to a few researchers. Moreover, the volume of data is growing rapidly as higher-resolution simulations are required to address the challenges posed by climate change, particularly extreme weather events. As the growth rate of the simulation data eclipses that of storage capacity, a shortage of storage space becomes inevitable (4, 5). As a result, there is an urgent need for data compression to store high-resolution simulation data while ideally having fast data access.

The exploration of data compression for weather and climate data starts with the lossless compression method (6–8) where data can be exactly restored after compression and decompression processes. However, they can hardly reach a high compression ratio above 6× for common atmospheric variables (8, 9) because they attempt to store the random noise component of the data, which is impossible to compress according to Shannon’s source coding theorem (10). In contrast, lossy compression allows for an approximation of the original data in exchange for significantly higher compression ratios. The simplest form of lossy compression is quantization, which represents a block of data with linearly scaled integers with lower number of bits than the original format. It is often used in conjunction with lossless compression methods to achieve higher compression ratios (11). Due to its simplicity, it is widely supported in modern scientific data formats such as NetCDF-4 (12), HDF5 (13), GRIB2 (14) and Zarr (15). Bit grooming (16) takes another approach of quantization by “shaving” the least significant bits of floating-point values to zeros. Bit rounding (17) extends this idea with the bit information criterion to determine the number of bits to shave off. Based on the quantization - lossless compression pipeline, transform-based methods such as JPEG (18), JPEG2000 (19) and SPECK (20) add a reversible transform before the quantization step to further increase the compression ratio. The SPERR (21) compressor extends SPECK with an outlier encoding layer to bound the maximum compression error. Variational autoencoders (22, 23) follow a similar pipeline as transform-based methods but replace the pre-defined transform with learned

## Significance Statement

High-resolution weather and climate simulations now generate petabytes of data, creating a storage crisis that bottlenecks research. We introduce EBCC, a novel error-bounded compressor that addresses this challenge with a two-layer compression approach: a base compression layer using JPEG2000 to capture the bulk of the data with a high compression ratio, and a residual compression layer using wavelet transform and Set Partitioning In Hierarchical Trees (SPIHT) encoding to efficiently eliminate long-tail extreme errors. We demonstrate its reliability across real-world applications. By enabling massive compression while preserving high fidelity, EBCC removes critical storage barriers, facilitating the analysis of next-generation climate models and democratizing access to large-scale environmental data for the broader scientific community.

Author affiliations: <sup>1</sup> Scalable Parallel Computing Laboratory, Department of Computer Science, ETH Zurich, Switzerland; <sup>2</sup> Institute for Atmospheric and Climate Science, Department of Environmental Systems Science, ETH Zurich, Switzerland; <sup>3</sup> Department of Applied Mathematics and Theoretical Physics, Centre for Mathematical Sciences, University of Cambridge, Cambridge, UK; <sup>4</sup> Microsoft Ibérica, Madrid, Spain

L.H., L.F., F.S., T.H. contributed to the implementation and experiment design. J.Z., M.A.S., S.S. contributed to the experiment design.

The authors declare no competing interest.

<sup>1</sup>To whom correspondence may be addressed. E-mail: torsten.hoefler@inf.ethz.ch

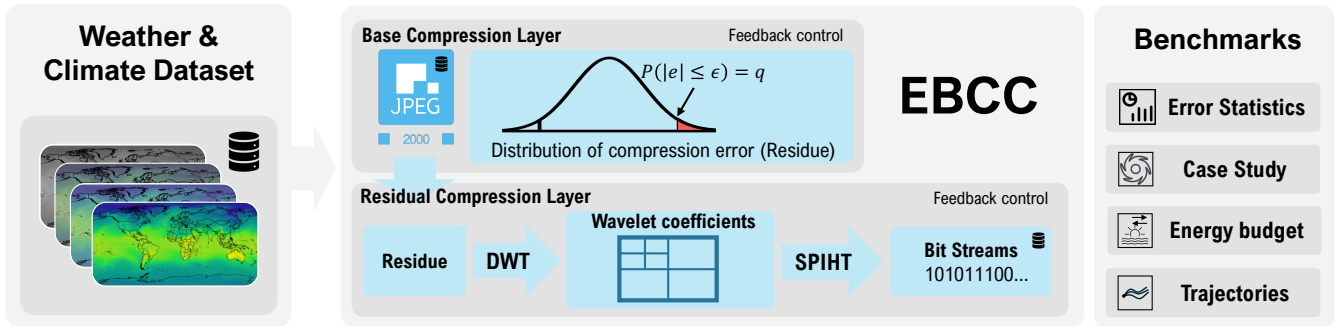


**Fig. 1.** Diagram of EBCC (Error Bounded Climate Compressor) method. It compresses weather & climate datasets using a two-layer approach: the base compression layer uses JPEG2000 for bulk compression, while the residual compression layer encodes excessive errors in the residue using discrete wavelet transform (DWT) and the set partitioning in hierarchical tree (SPIHT) algorithm. Both layers incorporate feedback control to achieve the target error bound. EBCC is evaluated on a suite of benchmarks and outperforms existing compression methods.

neural networks. Parallel to previous methods, prediction-based methods can achieve high compression ratios and max error bounded compression by estimating values from their neighbors and encoding the residuals. Examples include FPZIP (7), and the SZ family of methods (24–26). In addition, it is also possible to compress multidimensional data via tensor decomposition (27), or implicit neural representation (28).

Although lossy compression methods can achieve higher compression ratios than lossless ones, they introduce an additional complexity to the user due to the rate-distortion trade-off: users must decide a compression level where the resulting error metrics are acceptable for their applications. However, there is no consensus on the error metrics for weather and climate data. Point-wise metrics such as root-mean-square error (RMSE), peak signal-to-noise ratio (PSNR), and maximum absolute error are often used as the default metrics to evaluate compression errors. In addition, these metrics can be directly used as the error target in the compression methods. However, point-wise metrics oversimplify the compression errors as they ignore the correlation between neighboring data points. Baker et al. (29) suggests using the structural similarity index (SSIM) to evaluate the visual quality of the compressed climate data, and proposes a SSIM target of 0.99995 indicating visually indistinguishable data according to field experts. More statistical and visual metrics are proposed in Pinard et al. (30); Tintó Prims et al. (31). These metrics are useful when the compressed data is directly inspected by scientists or used as an end product, but they do not indicate the impact of downstream applications when the compressed data is used as input. Han et al. (22) evaluates the impact of compression on the forecasting skills of data-driven weather forecasting models. However, only one case study can hardly cover the whole field of weather and climate applications, and data-driven weather forecasting models are shown to be insensitive to small errors in the input data (32). We identify a gap in existing works that there lacks a comprehensive benchmark to evaluate compressed weather and climate data on representative applications.

Therefore, we create a benchmark suite for testing weather and climate applications on compressed datasets. It collects a wide range of test cases including error statistics, tropical cyclone case studies, energy budget closure analysis, and

Lagrangian air parcel trajectory simulation. The trajectory simulation benchmark, which traces the radioactive cloud of the Fukushima incident, is a novelty and proves to be an error-sensitive benchmark. We consider it to be a relevant test for compression methods in safety-critical applications.

With the benchmarks in mind, we introduce a new error-bounded compression method EBCC (Figure 1). It utilizes JPEG2000 in the base compression layer to optimize RMSE, a residual compression layer to eliminate long-tail extreme errors introduced by the base layer, and a feedback rate-control mechanism in both layers to achieve the specified maximum error target. We test our method alongside other established methods including SZ (24), SZ3 (25), SPERR (21), and Bitrounding (17). Our method outperforms all other methods across a wide range of compression ratios from 15× to more than 300×. It concentrates most errors near zero rather than distributing them uniformly within the error bound, resulting in less distortion in derived variables and simulated trajectories. It is capable of creating more than 100× compressed data while having downstream errors less than natural variability. Our contributions include:

- We create a novel error-bounded compressor that outperforms existing methods on weather and climate data.
- We create a comprehensive benchmark suite to test compression methods on weather and climate applications, including basic statistics, case studies on hurricane, energy budget closure, and Lagrangian trajectory simulations.
- We introduce ERA5 uncertainty ensembles as an indicator of natural variability for choosing error targets in practice, and show EBCC can achieve over 100× compression while keeping downstream errors within the natural variability.

## Benchmarks

We design a suite of benchmarks varying from compressing single-time-step sample data and collecting error statistics to using compressed data in complex applications inspired by real-world scenarios. In the first group of benchmarks, we apply compression on a small subset of the ERA5 dataset (33), and collect error statistics of the compression results including structural similarity (SSIM), histogram of point-wise errors, and power spectra of the reconstructed data. We further examine the visual quality of compressed data with a case

study in a tropical cyclone scenario. In addition to directly compressed variables, we compute horizontal divergence from compressed primitive variables to test the compressors' abilities of preserving relative values of neighboring locations and correlated variables. In the end, we apply the compressed data to a global energy budget closure analysis and a Lagrangian trajectory simulation as representative real-world applications. We also identify thresholds of compression errors suitable for practical use according to the natural variability represented by ERA5 uncertainty members.

Based on the benchmark suite, we test our method against other established compression methods: SZ, SZ3, SPERR, and Bitrounding. For error-bounded methods including SZ, SZ3, and SPERR, we vary the range-relative max absolute error tolerance from 0.1% to 10% to get a series of compressed data with varying compression ratios. Following Liang et al. (25), the range-relative max error is defined as the ratio of max absolute error and data range in a data chunk (see SI Table S1 for details). For Bitrounding, we vary the kept bit-wise information content from 80% to 99.9%. In energy balance analysis and Lagrangian trajectory simulation, we only benchmark EBCC and SZ3 since SZ3 has been leading in previous benchmarks.

**Table 1. Variables used in the benchmarks and sizes of related data stored in 32-bit floating-point format. u850 refers to zonal wind u at pressure level 850hPa, similar for v850 and u1000.**

Benchmark	Variables in Short Name	Raw Data Size
Error Statistics	z, t, q, u, v, w, u10, v10, t2m, msl	1.8 GB
Case Study	u850, v850, u1000, t2m	15.8 MB
Energy Closure	z, t, q, v, rsnt, r1nt, r1ns, rsns, hfss, hfls	111.0 GB
Trajectory Simulation	u, v, w, ps	6.1 GB

**Error Statistics.** We compress one-day sample data on 1st March 2024 with 10 pressure-level and surface-level variables (Table 1, Table 2). These variables represent the basic state of the atmosphere and are commonly used for weather forecasting (34). Figure 2 (left) shows the plot of compression ratio versus structural similarity (SSIM) for each compression method with relative error targets ranging from 0.1% to 10%, and annotates the 0.99995 SSIM threshold indicating the visually indistinguishable regime according to field experts (29). EBCC consistently outperforms other methods by having higher compression ratios at the same SSIM level. It can achieve a compression ratio of 35 $\times$  and maintain the SSIM above Baker's threshold at a 0.5% relative error target, while other methods can only achieve 10 $\times$  to 25 $\times$ .

We measure the compression and decompression throughput for each method as shown in Figure 2 (right). The throughput values are measured in single-thread on a desktop computer with an Intel Core i7-4770 CPU @ 3.4GHz and 2  $\times$  8GB DDR3 memory @ 1600 MHz. EBCC achieves a decompression throughput of 104.7 MB/s which is comparable to other methods (76.9 MB/s to 161.2 MB/s). It has a much lower compression throughput of 1.4 MB/s due to the overhead of double feedback loops. However, we can easily compress multiple data chunks in parallel to achieve a

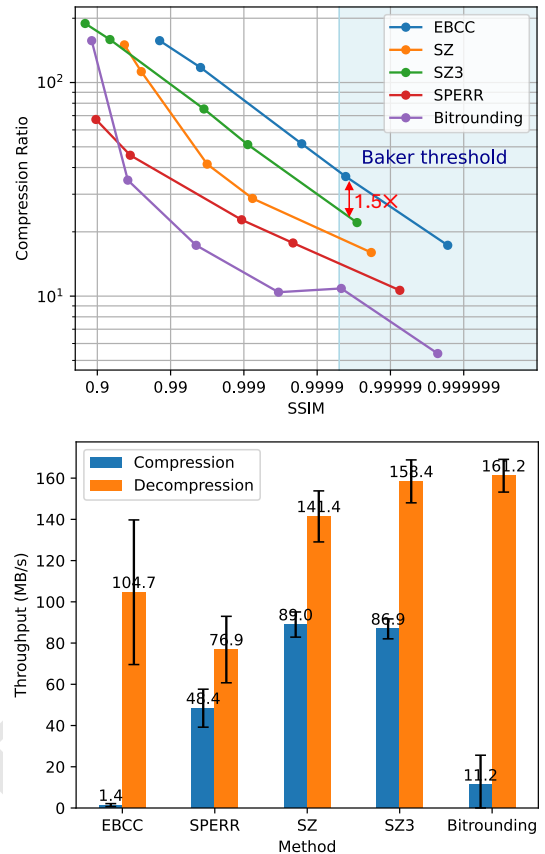


**Fig. 2. Top:** Rate-distortion plot of compression ratio (the higher the better) and structural similarity (SSIM, the higher the better) for a subset of ERA5 dataset (Table 1) with varying compression methods and parameters. The 0.99995 SSIM threshold proposed by Baker et al. (29) is marked on the plot. The numbers are grouped according to the compression method and error target (0.1%, 0.5%, 1%, 5%, 10%), and aggregated using harmonic mean for compression ratios and arithmetic mean for structural similarities over all variables, pressure levels, and timesteps. The values for the Bitrounding method are accumulated according to SSIM bins at [0.95, 0.9, 0.99, 0.999, 0.9999, 0.99999, 0.999999, 0.9999999]. **Bottom:** Compression and decompression throughput for each compression methods. The higher the better. The numbers are aggregated using arithmetic mean over all variables, pressure levels, timesteps and error targets. Error bars represent standard deviations of 1,140 samples.

higher throughput. Also, the compression throughput is not a critical factor in real-world applications since the weather data is usually compressed offline once and decompressed multiple times when accessed.

Furthermore, we examine the compression errors in histogram plots (Figure 3), and power spectra (Figure 4). In these plots, we select compressed data with compression ratios close to 10 $\times$  and 100 $\times$  by binary searching the error target (for EBCC, SZ, SZ3, and SPERR) and bit information (for Bitrounding). According to the error histogram of compressed 2m temperature in Figure 3, EBCC concentrates most errors towards 0 and has far fewer large errors compared with others. EBCC distributes errors close to a Gaussian distribution at a 10 $\times$  compression ratio, while the compression errors of other methods are more dispersed than the Gaussian distribution. SZ and SZ3 distribute errors close to a uniform distribution. As the compression ratio increases to 100 $\times$ , the distributions of errors are closer to the Gaussian distribution with the

**Table 2. Abbreviations of variables used in the benchmarks. TOA refers to top of atmosphere.**

Short Name	Long Name	Unit	Short Name	Long Name	Unit
<b>Pressure-level variables</b>					
z	Geopotential	$\text{m}^2\text{s}^{-2}$	t	Temperature	K
q	Specific humidity	$\text{kg kg}^{-1}$	u	Zonal wind	$\text{m s}^{-1}$
v	Meridional wind	$\text{m s}^{-1}$	w	Vertical velocity	$\text{Pa s}^{-1}$
<b>Surface variables</b>					
u10	10m zonal wind	$\text{m s}^{-1}$	v10	10m meridional wind	$\text{m s}^{-1}$
t2m	2m temperature	K	msl	Mean sea level pressure	Pa
ps	Surface pressure	Pa	rsnt	Net shortwave radiation at TOA	$\text{W m}^{-2}$
r1nt	Net longwave radiation at TOA	$\text{W m}^{-2}$	r1ns	Net longwave radiation at surface	$\text{W m}^{-2}$
rsns	Net shortwave radiation at surface	$\text{W m}^{-2}$	hfss	Surface sensible heat flux	$\text{W m}^{-2}$
hfls	Surface latent heat flux	$\text{W m}^{-2}$			

exception of Bitrounding, which has more negative errors than positive errors. Histogram plots of compression errors for other variables are available in the supporting information (Figure S1–S5), which show a similar trend as in Figure 3.

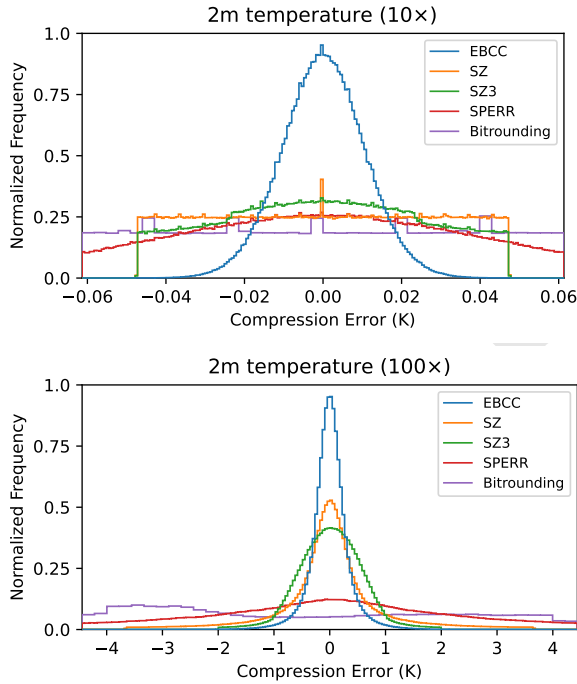


**Fig. 3.** Histogram of compression errors for 2m temperature ( $t_{2m}$ ) with compression ratios around  $10\times$  (top) and  $100\times$  (bottom). Each histogram is calculated on  $721 \times 1440$  samples. X-axis is cropped at the maximum compression error of EBCC. SPERR and Bitrounding have excessive errors in the cropped regions. They result in higher maximum errors while reaching a similar compression ratio as other methods.

In the spectra plots shown in Figure 4, we calculate the power of the spherical harmonic signal in each degree for both original and compressed geopotential data at 500hPa. We choose this variable because differences among methods are more distinctive, and features observed in Figure 4 also apply to other variables (available in the SI Figure S6–S10). In the high accuracy regime with a compression ratio of  $10\times$  (left), all the compression methods perform well by having

almost identical spectra as the reference one. When zooming in the high-frequency region, EBCC and Bitrounding are closest to the reference, and other methods add artificial high-frequency components to the compressed data. In the high compression ratio regime with a compression ratio of  $100\times$  (right), EBCC and SZ3 still conform well to the reference while others add significant medium-to-high frequency artifacts. EBCC slightly underestimates high-frequency details which effectively smooths the data, but it does not introduce high frequency artifacts in any case unlike SZ3 (see in SI Appendix). We will further inspect compressed data in the following section.

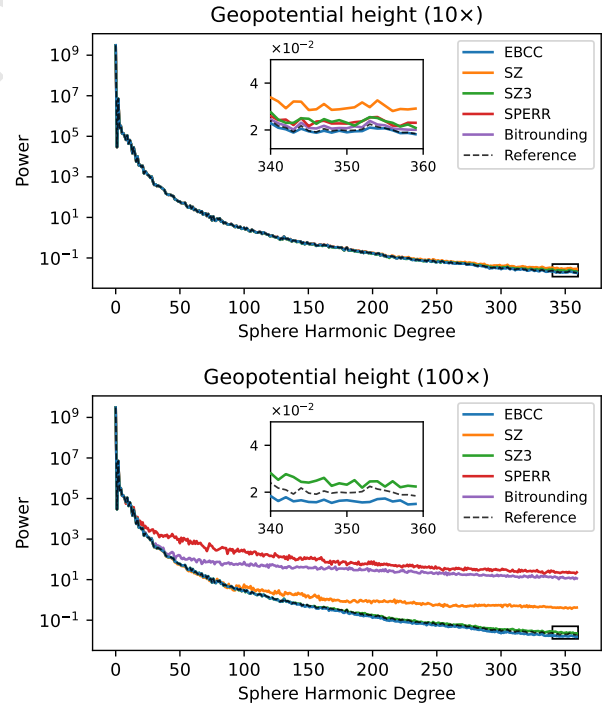


**Fig. 4.** Spherical harmonics power spectra of compressed and original data for geopotential ( $z$ ) at 500hPa with compression ratios around  $10\times$  (top) and  $100\times$  (bottom). Each power spectrum is calculated on a  $721 \times 1440$  grid.

**Case Study of Hurricane Iota.** Weather and climate data are often used for visual examination, thus it is important for

compressors to preserve the visual fidelity of the compressed data. To test this, we select the data containing the record-breaking hurricane Iota on 16th Nov 2020. We use binary search to find the right compression parameters that produce 10× and 100× compressed data. Due to the constraint of the Bitrounding method, it cannot achieve a high compression ratio larger than 17×. In Figure 5, all of the compressed data are perceptually similar to the reference with a compression ratio of 10×. When relaxing to 100×, SZ produces obvious blocked artifacts, SPERR reduces the data into several regions with distinct values, SZ3 introduces some mild bumps. EBCC smoothens some details around the hurricane, but it does not add any artifacts. The residue plot in Figure 5 bottom verifies this observation. In addition, it shows EBCC has an edge over SZ3 because the compression errors of EBCC are lower in magnitude and have lower low-frequency component.

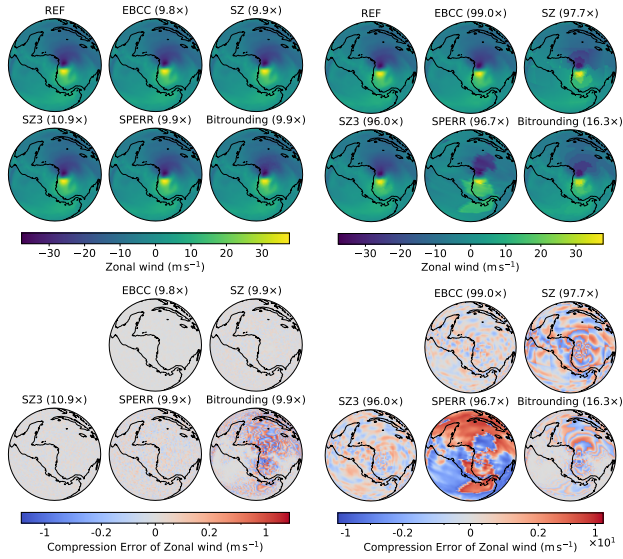


**Fig. 5. Top:** Plots of compressed 850hPa zonal wind speed ( $u$ ) of hurricane Iota with compression ratios around 10× (left) and 100× (right). **Bottom:** Plots of compression errors with corresponding compression ratios as top plots.

While compression methods including EBCC, SZ, and SZ3 can preserve visual features of compressed data even at a high compression ratio of 100×, this is less likely when examining derived variables computed from compressed primitive variables. Figure 6 shows the derived 850hPa horizontal wind divergence at the hurricane location. Horizontal divergence is calculated from the spatial derivatives of two components of horizontal wind speed. Compressors have to reconstruct the first order spatial derivatives accurately to maintain a good fidelity of computed divergence. At a compression ratio of 10×, there are noticeable degradations for Bitrounding compressed data. Others are close to the reference with EBCC producing the least errors. At a compression ratio of 100×, EBCC results in a slightly blurred image, SZ3 introduces high-frequency dot-like artifacts, while SZ and SPERR produce near incomprehensible results. Bitrounding produces low-quality horizontal divergence albeit at a 14.5× compression ratio.

**Energy Budget Closure Analysis.** It is important to maintain the physical consistency of the compressed data. In

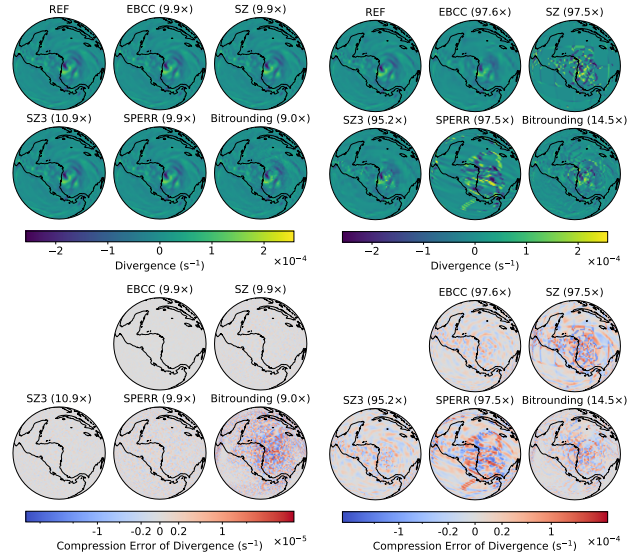


**Fig. 6. Top:** Plots of derived 850-hPa horizontal wind divergence from compressed horizontal winds with compression ratios around 10× (left) and 100× (right). **Bottom:** Plots of compression errors with corresponding compression ratios as top plots.

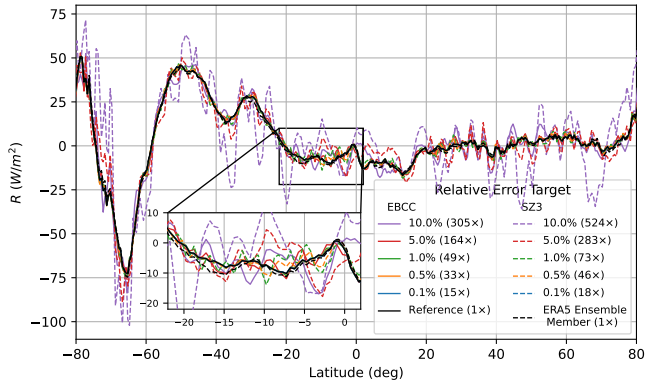


**Fig. 7.** Monthly zonal mean energy budget residual  $R$  for compressed and original data for September 2016. The relative error target is set to 0.1%, 0.5%, 1%, 5%, and 10% respectively. The resulting compression ratios are marked in the legend.

the previous benchmark, we have tested a simple case of calculating wind divergence. In this section, we perform a more complex benchmark by testing the closure of the global atmospheric energy budget using compressed data. In essence, this benchmark examines the deviation in the sum of compressed data in an attempt to reproduce atmospheric heat transport derived from 3D atmospheric fields. Ideally, we expect compression errors to be zero-centered, thus not adding bias to statistics such as spatial or temporal mean. The zonal mean moist static energy (MSE) framework is a commonly used approximation of the atmospheric energy budget which has been used to study the Arctic climate (35) or storm track shifts (36). At a given latitude band, there is a balance in the energy fluxes:

$$R := \partial_t \langle [\bar{h}] \rangle + \partial_y \langle [\bar{v}m] \rangle - \overline{[F_{NE}]} \approx 0 \quad [1]$$

(37). The first term on the left-hand side corresponds to the tendency of the thermal energy within the atmospheric

column,  $h = c_p T + Lq$ , with  $c_p$  the specific heat capacity of dry air and  $L$  the latent heat of evaporation, which are both taken as constant here.  $T$  and  $q$  are air temperature and specific humidity, respectively. The second term denotes the meridional divergence of the flux of MSE that is the product of the meridional wind,  $v$ , and  $m = c_p T + Lq + \Phi$  with  $\Phi$  the geopotential. The third term represents the net energy (NE) input into the column by surface and top of atmosphere radiative and turbulent heat fluxes. Square brackets denote zonal averages and angle brackets the mass-weighted vertical integration using climatological mean surface pressure (38). The overbars denote temporal averaging the data over a month. Note that the goal is to evaluate the compression with respect to a heat budget diagnostic that is comparably simple to apply and thus broadly used in the field (as for instance in 39) instead of more sophisticated approaches (40). This comprehensive combination of operations and variables helps us better understand the effect of compression in a real-world scenario. We make use of 111 gigabytes of  $1^\circ$ -resolution ERA5 data from August to October 2016 to calculate the terms in Equation 1 for September 2019. Then we compress the data with relative error targets of 0.1%, 0.5%, 1%, 5%, and 10% respectively, and compute the zonal mean energy budget residual  $R$  for the original and compressed data. Perfect budget closure would correspond to a vanishing residual  $R \equiv 0$ . The computed residual has the order of  $\approx 15 \text{ W m}^{-1}$  (black line in Figure 7) which is in line with other previous estimates (41, 42) and within the typical range of different turbulent surface heat flux estimates (43). A considerable fraction of this residual can be linked to uncertainties in assimilated surface heat fluxes (44). Simplifications in the method following (42, 45, 46) further introduce discrepancies, particularly over the steep Antarctic topography near  $70^\circ \text{ S}$ . Turning to the evaluation of the compression algorithms, this reference residual serves as a benchmark for the performance of the compression algorithms. In other words, deviations from the reference should ideally be small compared to the reference residual itself.

As shown in Figure 7,  $R$  computed from compressed data is close to the reference except for SZ3 with 5% and 10% relative error targets. These two cases result in significant differences in  $R$  although achieving high compression ratios of 283 $\times$  and 524 $\times$ . In contrast,  $R$  computed from EBCC compressed data is closer to the reference. Quantitatively, we calculate the RMSE of  $R$  for the compressed data and plot the rate-distortion plot for EBCC and SZ3 (Figure 8 left). It is clear that EBCC outperforms SZ3 in RMSE at compression ratios ranging from 20 $\times$  to 300 $\times$ , while EBCC typically allows a higher error bound compared with SZ3 to achieve the same compression ratio. In the plot, we highlight the RMSE due to ERA5 uncertainty representing the natural variability. It is created by running the benchmark on each of the 10 members representing ERA5 uncertainty and taking the largest RMSE of the 10 members. It can help decide the error target or compression ratio for lossy compression. In this case, EBCC can reach a 100 $\times$  compression ratio with resulting errors within natural variability, while SZ3 can only reach 50 $\times$ .

In the right plot of Figure 8, we show the cumulative distribution function (CDF) of absolute errors of  $R$ , representing the fraction of errors whose absolute value is larger than a

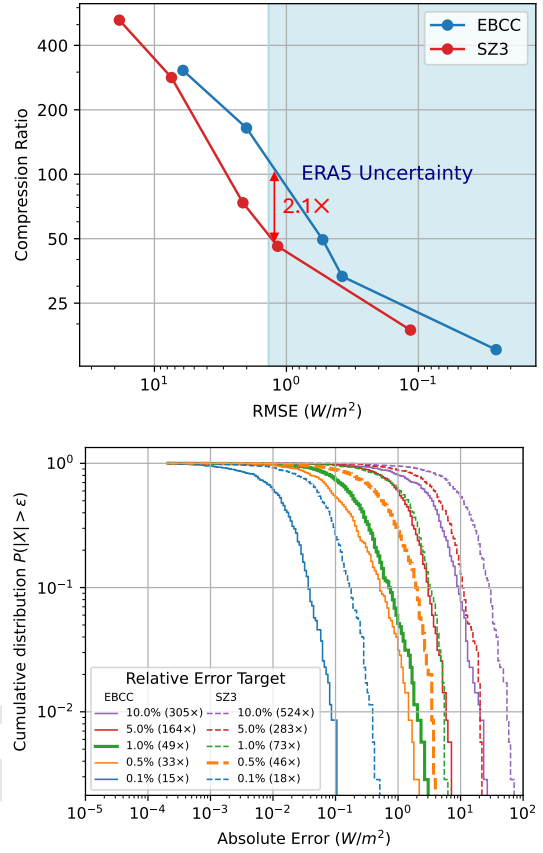


**Fig. 8. Top:** Line plot of compression ratio and RMSE of compressed  $R$  (rate-distortion plot). **Bottom:** Cumulative distribution function (CDF) of absolute errors of  $R$  induced by compression. Each CDF is calculated on 180 samples. EBCC with 1% relative error target and SZ3 with 0.5% error target are highlighted. EBCC's CDF dominates SZ3's despite of having similar compression ratios (49 $\times$  and 46 $\times$ ).

certain value. The CDFs for EBCC are smaller than SZ3's at the same relative error target, indicating that EBCC has a smaller portion of large errors. This even holds true when the two have similar compression ratios (e.g., EBCC 1% and SZ3 0.5% relative error target). In sum, EBCC is the preferable choice to conserve the zonal mean energy budget terms at a monthly scale.

**Lagrangian Trajectory Simulation.** In the end, we present the Lagrangian air parcel trajectory simulation as a formidable benchmark. Trajectories are highly sensitive to errors in the wind data, and small errors in the beginning will amplify in following time as the simulator integrates wind speeds at the positions of the air parcels. We design an experiment simulating the trajectories of air parcels around the Fukushima nuclear incident for one week using the Lagrangian analysis tool LAGRANTO (47), and examine the deviation of trajectories caused by using compressed wind data. Similar to the energy budget benchmark, we run trajectory simulations on ERA5 uncertainty members and take the smallest error metric of all the members to estimate the natural variability of the data.

The deviation of trajectories is measured through the RMSE of particle densities at every time step, where we treat each tracked air parcel as an abstract particle. This

effectively measures the difference of the particle distribution. Figure 9 shows the rate-distortion plot for EBCC and SZ3. EBCC has approximately  $1.9\times$  compression ratio of SZ3 at the same RMSE level. Similarly, it can achieve around 50% RMSE at the same compression ratio. The baseline RMSE derived from trajectories of ERA5 uncertainty members is relatively high. This allows a 10% error target for EBCC and 1% - 5% error target for SZ3, which results in compression ratios of  $282\times$  and around  $150\times$  respectively.

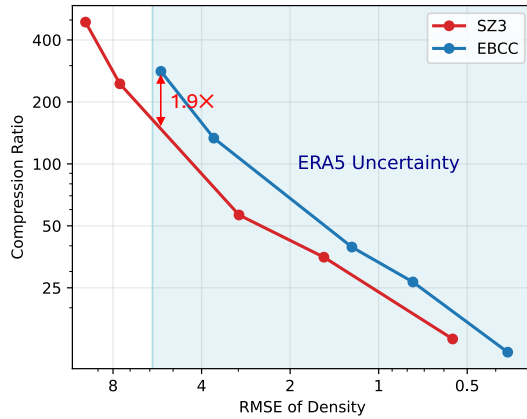


Fig. 9. Line plot of compression ratio and RMSE of particle densities at every timestep (rate-distortion plot).

Figure 10 shows the simulated trajectory using original, ERA5 uncertainty ensemble member, and compressed data. We select EBCC with relative error targets of 10% and 1%, and SZ3 with targets of 5% and 0.5%, since the two pairs have similar compression ratios. As indicated in Figure 9, the difference between trajectories of ERA5 ensemble members is evident, as more lower level particles circle around the north-western Pacific in member 1. EBCC with 1% relative error results in a similar trajectory plume as the reference with only a slight change in the thickness of low level ( $> 950\text{hPa}$ ) trajectories around  $50^\circ\text{N}$ ,  $160^\circ\text{E}$ . When relaxing the error target to 10%, the changes in near-surface trajectories (green and yellow) become more apparent while there are fewer trajectories going north at higher levels (blue). For SZ3, the difference in trajectories at 0.5% relative error is already comparable to EBCC at 1% relative error. The trajectories for SZ3 with 5% relative error are visibly different from the reference trajectories with ERA5 member 0 data and such difference is larger than the difference between ensemble members. In Figure 11, we examine the density of tracked particles one week after the Fukushima incident. Both EBCC at 1% and SZ3 at 0.5% relative error targets produce perceptually similar distributions as the reference. At 10% error target, our method keeps the general distribution, while SZ3 at 5% error target results in fewer air parcels near the south-east region of the Kamchatka peninsula and the US west coast. In summary, EBCC can produce a compressed wind field, introducing less error in simulated trajectories compared with SZ3 at the same compression ratios. It can achieve a  $282\times$  compression ratio while keeping induced errors below that of ERA5 uncertainty.

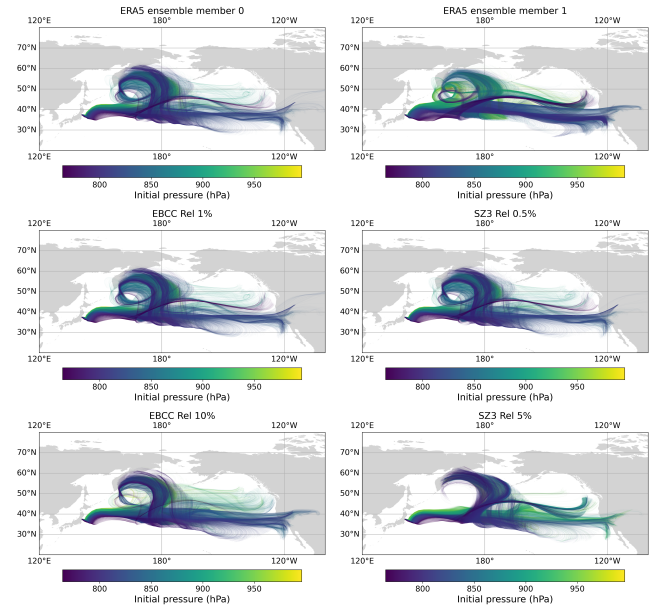
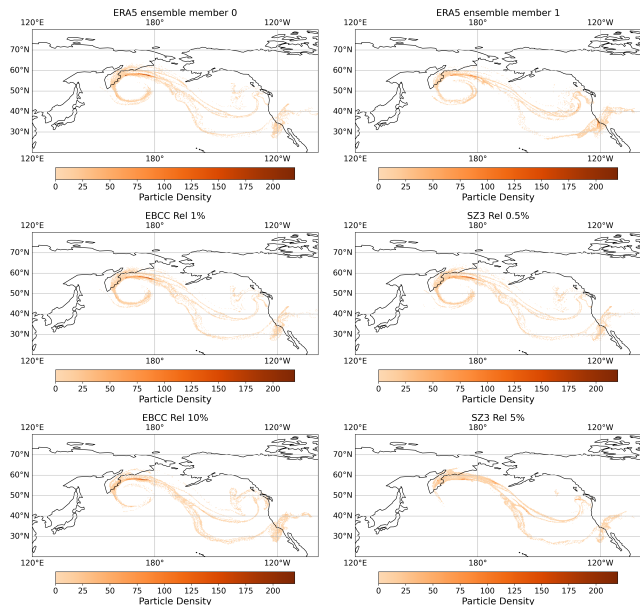


Fig. 10. Simulated trajectories of particles around the Fukushima incident in 1 week period colored by the initial pressure level of particles. The simulations are performed with original wind speed data from ERA5 (ensemble member 0), ERA5 uncertainty ensemble member 1, compressed data with EBCC relative error targets at 1% and 10% (compression ratio:  $39\times$ ,  $282\times$ ), and SZ3 relative error targets at 0.5% and 5% (compression ratio:  $35\times$ ,  $245\times$ ).

## Conclusion

This study introduces a novel error-bounded compression method EBCC targeted for weather and climate data. It contains a base compression layer using JPEG2000 to capture the bulk of the data and a residual compression layer to record the sparse signal that exceeds the given error bound. The residual compression layer encodes the residue of the previous layer using the SPIHT algorithm. We also introduce feedback-based rate control for both layers that adjusts the compression ratios to achieve the given error bound. We implement EBCC as a standalone C library with CDO and Zarr plugins, which transparently integrates into existing toolchains.

We test EBCC with established compression methods on a suite of benchmarks including error statistics, a case study of a tropical cyclone, the closure of the Earth's energy budget, and a Lagrangian air parcel trajectory simulation. EBCC is superior in all benchmark cases at given range relative error targets from 0.1% to 10% and compression ratios from  $16\times$  to more than  $300\times$ , respectively. Our method can reconstruct the derivatives of the compressed data with high fidelity. As the compression ratio or error bound increases, the EBCC compressed data degrades to a smoothed dataset instead of adding high-frequency artifacts found in other compression methods. In energy balance analysis and Lagrangian trajectory simulations, EBCC results in less distortion compared to the best existing method SZ3 at comparable compression ratios. It can achieve more than  $100\times$  compression ratios while keeping downstream error metrics within natural variability derived from ERA5 uncertainty members. EBCC is an important step forward to cope with the growing difficulties in storing weather and climate data.



**Fig. 11.** Density of simulated particles 1 week after the Fukushima incident. The simulations are performed with original wind speed data from ERA5 (ensemble member 0), ERA5 uncertainty ensemble member 1, compressed data with EBCC relative error targets at 1% and 10% (compression ratio:  $39\times$ ,  $282\times$ ), and SZ3 relative error targets at 0.5% and 5% (compression ratio:  $35\times$ ,  $245\times$ ). There are 35,298 simulated particles in each simulation.

**Code Availability.** The source code of EBCC is available in [github.com/spcl/EBCC](https://github.com/spcl/EBCC).

## Materials and Methods

To compress weather data with EBCC, we split the four-dimensional input array (time, level, latitude, longitude) into multiple chunks of the same shape and encode each chunk separately. Note that the implementation of EBCC supports arbitrary multidimensional arrays. We adapt the four-dimensional-array interpretation for the sake of the benchmark. Next, each chunk is flattened into a two-dimensional array. For example, an array of shape  $(T, P, H, W)$  is flattened into  $(T \times P \times H, W)$ . Then the 2D array is normalized according to its minimum and maximum values and fed to the EBCC compressor following the [algorithm 1](#). Inside, the data is firstly compressed by the base compression layer using a JPEG2000 codec. JPEG2000 can compress data with a near-optimal RMSE under a given compression ratio, but it can result in long-tail errors which are problematic for weather data, in particular extreme weather events. Therefore, we add a second residual compression layer to keep overall compression error within a specific error bound. Unlike SPERR which directly encodes in the spatial domain, our method transforms the residue into wavelet coefficients and encodes the coefficients using the SPIHT algorithm ([48](#)). The SPIHT algorithm goes through the bit planes of the wavelet coefficients from the most significant to the least significant plane and encodes significant bits in each bit plane. The residues related to excessive errors are likely encoded earlier, and therefore can be compressed with a high compression ratio. In fact, it creates an embedded code sequence where any prefix is also a valid sequence. Thanks to this property, we can easily control the compression rate by truncating the generated sequence.

While the two layer compression approach provides a flexible way to compress data with a near-optimal RMSE while maintaining a maximum absolute error bound, there is no direct way to determine the compression ratio as the compression parameter a priori given an error bound. Instead, we use feedback loops to find a suitable compression ratio iteratively. Since the base compression layer should compress the bulk part of the data while only leaving a small portion of excessive values to the sparse

wavelet compression layer, we set a parameter  $q$  to quantify the "small portion", and control the base compression ratio so that the portion of non-excessive errors is  $q$ . In other words, the error bound is equal to the  $q$ -quantile of the compression error. Similarly, with base compression fixed, we perform a single SPIHT encoding of the wavelet-transformed residue, and binary search the lowest truncation point that satisfies the error bound. We use binary search in feedback loops because it requires approximately 4 iterations to converge in practice, and replacing it with more complex searching algorithms does not improve performance. Since the residual compression layer is designed for sparse excessive errors, the two-layer approach is suboptimal when the base compression alone can compress within the desired max error bound. In that case, a fallback mechanism at the end of [algorithm 1](#) returns the data compressed using the base compression alone (equivalent to setting  $q = 1$ ), if it creates a higher compression ratio. This ensures EBCC is always better than or equal to the base compression alone.

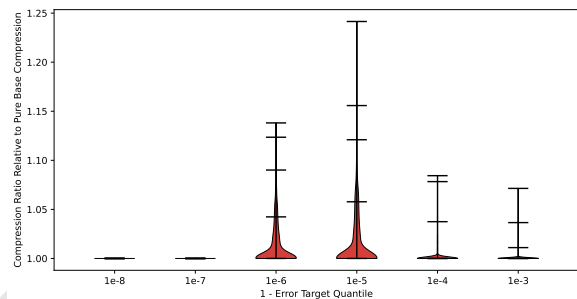


**Fig. 12.** Violin plot showing the distributions of EBCC's compression ratios (1,140 samples) for different parameter  $q$ . The compression ratios are presented relative to using pure base compression (JPEG2000) only ( $q = 1$ ). Horizontal ticks in the violin plot represent maximum value, 0.999, 0.99, and 0.9 quantiles.

**Implementation Details.** We implement EBCC as a C library using OpenJPEG as the JPEG2000 codec and a custom SPIHT encoder following [imshrinker\(49\)](#). It currently supports single-precision floating-point input values and can be easily extended to other number formats. We also wrap the C library into an HDF5 filter plugin ([13](#)) to support compression and decompression of HDF5 datasets. In addition, it enables transparent decompression for tools supporting the HDF5 format, including NetCDF ([12](#)), NCO ([50](#)), CDO ([51](#)), or xarray ([52](#)).

In the benchmark, we utilize the SZ, SZ3, and SPERR compression plugins from [hdf5plugin\(53\)](#) to produce compressed NetCDF files and use [enstools-compression\(31\)](#) to automate the compression and decompression process.

**Ablation Study.** We introduce a parameter  $q$  in EBCC to control the amount of excessive errors left for the residue compression layer. The optimal value of  $q$  is dependent on the input data. If the input data is very smooth, we can set  $q = 1$  since the base compression layer alone can compress it without introducing excessive errors. On the other hand, if the input data contains outliers that are smoothed out by the base compression layer, we can decrease  $q$  to let the residual compression layer encode an increasing portion of outliers. We perform an ablation study to investigate the effects of varying  $q$  when compressing weather and climate data. In the ablation study, we compress a sample ERA5 dataset with the same configuration as the error statistics benchmark while varying  $q$  from  $1 - 10^{-3}$  to 1 and range relative max error bound from 0.1% to 10%. We compress each 2D slice of the sample dataset and calculate the relative compression ratio compared with  $q = 1$ .

In [Figure 12](#), we collect the relative compression ratios for different  $q$  values, and plot their distribution. In every case, the relative compression ratios are larger than or equal to 1, thanks to the pure base compression fallback mechanism. The residual compression layer is most effective when  $q$  ranges from  $1 - 10^{-5}$  to  $1 - 10^{-6}$ . It can improve the compression ratio by up to 24% compared with pure base compression. However, when  $q$  is outside of the range, the relative compression ratios converge to 1 because

---

**Algorithm 1: EBCC Compression Process**

---

**Input:** 2D array  $A$ , max error target  $\epsilon$ , initial base compression ratio  $r_0$ , proportion  $q$  that base compression errors do not exceed  $\epsilon$ .

**Output:** Compressed byte sequence  $e$ , can be decompressed with error less than  $\epsilon$ .

**Auxiliary functions:** Encoding and decoding function of base compression method  $\text{enc}_{\text{base}}$ ,  $\text{dec}_{\text{base}}$ , discrete wavelet transformation DWT and its inverse IDWT, and encoding and decoding function of SPIHT  $\text{enc}_{\text{SPIHT}}$ ,  $\text{dec}_{\text{SPIHT}}$ .

**Function**  $\text{enc}_{\text{base}}(A, r, \epsilon)$

```
 $e_A \leftarrow$  Compressed data of applying base compression method to  $A$  with a compression ratio  $r$ ;  
 $q_A \leftarrow$  Proportion of compression errors that do not exceed  $\epsilon$ ;  
return  $e_A, q_A$ ;
```

**end**

// Choose valid CR range for binary search

```
 $e_A, q_{A0} \leftarrow \text{enc}_{\text{base}}(A, r_0, \epsilon)$ ;
```

```
 $r_{\text{low}} \leftarrow r_0, r_{\text{high}} \leftarrow r_0$ ;
```

```
 $q_A \leftarrow q_{A0}$ ;
```

```
while  $q_A \geq q$  do // Initial CR too high
```

```
   $r_{\text{low}} \leftarrow r_{\text{low}}/2$ ;
```

```
   $e_A, q_A \leftarrow \text{enc}_{\text{base}}(A, r_{\text{low}}, \epsilon)$ ;
```

**end**

```
 $e_f \leftarrow e_A$ ;
```

```
 $q_A \leftarrow q_{A0}$ ;
```

```
while  $q_A \leq q$  do // Initial CR too low
```

```
   $r_{\text{high}} \leftarrow r_{\text{high}} * 2$ ;
```

```
   $e_A, q_A \leftarrow \text{enc}_{\text{base}}(A, r_{\text{high}}, \epsilon)$ ;
```

**end**

// Binary search for best feasible CR

```
 $\text{tol} \leftarrow 10^{-3}$ ;
```

```
while  $r_{\text{high}} - r_{\text{low}} > \text{tol}$  do
```

```
   $r_{\text{mid}} \leftarrow (r_{\text{low}} + r_{\text{high}})/2$ ;
```

```
   $e_A, q_A \leftarrow \text{enc}_{\text{base}}(A, r_{\text{mid}}, \epsilon)$ ;
```

```
  if  $q_A < q$  then
```

```
     $r_{\text{high}} \leftarrow r_{\text{mid}}$ ;
```

```
  else
```

```
     $r_{\text{low}} \leftarrow r_{\text{mid}}$ ;
```

```
     $e_f \leftarrow e_A$ ;
```

```
  end
```

**end**

```
 $e_{\text{base}} \leftarrow e_f$ ;
```

```
 $A_{\text{base}} \leftarrow \text{dec}_{\text{base}}(e_{\text{base}})$ ;
```

```
 $A_{\text{residue}} \leftarrow A - A_{\text{base}}$ ;
```

```
 $W_A \leftarrow \text{DWT}(A_{\text{residue}})$ ;
```

```
 $e_{\text{SPIHT}} \leftarrow \text{enc}_{\text{SPIHT}}(W_A)$ ;
```

```
 $t_{\text{low}} \leftarrow 0, t_{\text{high}} \leftarrow \text{len}(e_{\text{SPIHT}})$ ;
```

// Binary search for best feasible truncation point

```
while  $t_{\text{high}} - t_{\text{low}} > \text{tol}$  do
```

```
   $t_{\text{mid}} \leftarrow (t_{\text{low}} + t_{\text{high}})/2$ ;
```

```
   $A_{\text{rec}} \leftarrow \text{IDWT}(\text{dec}_{\text{SPIHT}}(e_{\text{SPIHT}}[t_{\text{mid}}])) + A_{\text{base}}$ ;
```

```
  if  $\max(|A - A_{\text{rec}}|) > \epsilon$  then
```

```
     $t_{\text{low}} \leftarrow t_{\text{mid}}$ ;
```

```
  else
```

```
     $t_{\text{high}} \leftarrow t_{\text{mid}}$ ;
```

```
  end
```

**end**

```
 $e_{\text{residue}} \leftarrow e_{\text{SPIHT}}[t_{\text{high}}]$ ;
```

```
 $e \leftarrow \text{Concat}(e_{\text{base}}, e_{\text{residue}})$ ;
```

```
return  $e$ 
```

// Compressed byte sequence

---

the residual compression layer either encodes too much data that it becomes less efficient than the base compression layer, resulting in a pure compression fallback, or it does not receive enough data as the base compression layer simply compresses all the data when  $q$  is too close to 1. As a result, we set  $q = 1 - 10^{-5}$  in the following benchmarks.  $q$  might need to be tuned when having a different dataset to get an optimal compression ratio.

## ACKNOWLEDGMENTS.

This work received funding from the WeatherGenerator project (grant agreement No 101187947). It was supported under project ID a01 and a122 as part of the Swiss AI Initiative, through a grant from the ETH Domain and computational resources provided by the Swiss National Supercomputing Centre (CSCS) under the Alps infrastructure. We also thank CSCS for the provisioning of compute resources for this project.

1. P Bauer, et al., The digital revolution of earth-system science. *Nat. Comput. Sci.* **1**, 104–113 (2021).
2. MC Acosta, et al., The computational and energy cost of simulation and storage for climate science: lessons from cimp6. *Geosci. Model. Dev.* **17**, 3081–3098 (2024).
3. M Govett, et al., Exascale computing and data handling: Challenges and opportunities for weather and climate prediction. *Bull. Am. Meteorol. Soc.* **105**, E2385–E2404 (2024).
4. T Hoefler, et al., Earth virtualization engines: a technical perspective. *Comput. Sci. & Eng.* **25**, 50–59 (2023).
5. ECMWF, Annual report 2023 (2023) Accessed: 2024-04-22.
6. RF Rice, Lossless coding standards for space data systems in *Conference Record of the Thirtieth Asilomar conference on Signals, Systems and Computers.* (IEEE), Vol. 1, pp. 577–585 (1996).
7. PG Lindstrom, Fzip, (Lawrence Livermore National Laboratory (LLNL), Livermore, CA (United States)), Technical report (2017).
8. X Huang, et al., Czip: A fast lossless compression algorithm for climate data. *Int. J. Parallel Program.* **44**, 1248–1267 (2016).
9. BC MummadiSETTY, A Puri, E Sharifahmadian, S Latifi, Lossless compression of climate data in *Progress in Systems Engineering: Proceedings of the Twenty-Third International Conference on Systems Engineering.* (Springer), pp. 391–400 (2015).
10. CE Shannon, A mathematical theory of communication. *The Bell system technical journal* **27**, 379–423 (1948).
11. JD Silver, CS Zender, The compression–error trade-off for large gridded data sets. *Geosci. Model. Dev.* **10**, 413–423 (2017).
12. Unidata, NetCDF-C Library (2025).
13. M Folk, A Cheng, K Yates, Hdf5: A file format and i/o library for high performance computing applications in *Proceedings of supercomputing.* Vol. 99, pp. 5–33 (1999).
14. WMO, *Manual on Codes – Volume I.2: FM 92 GRIB, Edition 2* (World Meteorological Organization, Geneva, Switzerland), (2025) WMO-No. 306; valid 19 May 2025.
15. A Miles, J Kirkham, JJ Hamman, , et al., zarr-python: v2.18.5 (2025).

16. CS Zender, Bit grooming: statistically accurate precision-preserving quantization with compression, evaluated in the netcdf operators (ncf, v4. 4.8+). *Geosci. Model. Dev.* **9**, 3199–3211 (2016).
17. M Klöwer, M Razingger, JJ Dominguez, PD Düben, TN Palmer, Compressing atmospheric data into its real information content. *Nat. Comput. Sci.* **1**, 713–724 (2021).
18. GK Wallace, The JPEG Still Picture Compression Standard. *Commun. ACM* **34**, 30–44 (1991).
19. ISO Central Secretary, Information technology — jpeg 2000 image coding system part 1: Core coding system, (International Organization for Standardization, Geneva, CH), Standard ISO/IEC 15444-1:2024 (2024).
20. Cc Chao, RM Gray, Image compression with a vector speck algorithm in *2006 IEEE International Conference on Acoustics Speech and Signal Processing Proceedings.* (IEEE), Vol. 2, pp. II-II (2006).
21. S Li, P Lindstrom, J Clyne, Lossy scientific data compression with sperr in *2023 IEEE International Parallel and Distributed Processing Symposium (IPDPS).* pp. 1007–1017 (2023).
22. T Han, Z Chen, S Guo, W Xu, L Bai, Cra5: Extreme compression of era5 for portable global climate and weather research via an efficient variational transformer. *arXiv preprint arXiv:2405.03376* (2024).
23. P Mirowski, et al., Neural compression of atmospheric states. *arXiv preprint arXiv:2407.11666* (2024).
24. S Di, F Cappello, Fast error-bounded lossy hpc data compression with sz in *2016 IEEE international parallel and distributed processing symposium (ipdps).* (IEEE), pp. 730–739 (2016).
25. X Liang, et al., Sz3: A modular framework for composing prediction-based error-bounded lossy compressors. *IEEE Transactions on Big Data* **9**, 485–498 (2022).
26. Z Jian, et al., Cliz: Optimizing lossy compression for climate datasets with adaptive fine-tuned data prediction in *2024 IEEE International Parallel and Distributed Processing Symposium (IPDPS).* (IEEE), pp. 417–429 (2024).

27. R Ballester-Ripoll, P Lindstrom, R Pajarola, Tthresh: Tensor compression for multidimensional visual data. *IEEE transactions on visualization computer graphics* **26**, 2891–2903 (2019).
28. L Huang, T Hoefler, Compressing multidimensional weather and climate data into neural networks. *arXiv preprint arXiv:2210.12538* (2022).
29. AH Baker, DM Hammerling, TL Turton, Evaluating image quality measures to assess the impact of lossy data compression applied to climate simulation data in *Computer Graphics Forum*. (Wiley Online Library), Vol. 38, pp. 517–528 (2019).
30. A Pinard, DM Hammerling, AH Baker, Assessing differences in large spatio-temporal climate datasets with a new python package in *2020 IEEE International Conference on Big Data (Big Data)*. (IEEE), pp. 2699–2707 (2020).
31. O Tintó Prims, et al., The effect of lossy compression of numerical weather prediction data on data analysis: a case study using enstools-compression 2023.11. *Geosci. Model. Dev.* **17**, 8909–8925 (2024).
32. T Selz, GC Craig, Can artificial intelligence-based weather prediction models simulate the butterfly effect? *Geophys. Res. Lett.* **50**, e2023GL105747 (2023).
33. H Hersbach, et al., The era5 global reanalysis. *Q. journal royal meteorological society* **146**, 1999–2049 (2020).
34. S Rasp, et al., Weatherbench: a benchmark data set for data-driven weather forecasting. *J. Adv. Model. Earth Syst.* **12**, e2020MS002203 (2020).
35. RG Graversen, M Burtu, Arctic amplification enhanced by latent energy transport of atmospheric planetary waves. *Q. J. Royal Meteorol. Soc.* **142**, 2046–2054 (2016).
36. TA Shaw, P Barpanda, A Donohoe, A moist static energy framework for zonal-mean storm-track intensity. *J. Atmospheric Sci.* **75**, 1979–1994 (2018).
37. JD Neelin, IM Held, Modeling tropical convergence based on the moist static energy budget. *Mon. Weather. Rev.* **115**, 3–12 (1987).
38. GJ Boer, NE Sargent, Vertically integrated budgets of mass and energy for the globe. *J. Atmospheric Sci.* **42**, 1592–1613 (1985).
39. J Marshall, A Donohoe, D Ferreira, D McGee, The ocean’s role in setting the mean position of the inter-tropical convergence zone. *Clim. Dyn.* **42**, 1967–1979 (2014).
40. J Mayer, M Mayer, L Haimberger, Consistency and homogeneity of atmospheric energy, moisture, and mass budgets in era5. *J. Clim.* **34**, 3955–3974 (2021).
41. KE Trenberth, JT Fasullo, J Mackaro, Atmospheric moisture transports from ocean to land and global energy flows in reanalyses. *J. climate* **24**, 4907–4924 (2011).
42. M Mayer, L Haimberger, JM Edwards, P Hyder, Toward consistent diagnostics of the coupled atmosphere and ocean energy budgets. *J. Clim.* **30**, 9225–9246 (2017).
43. HD Prince, A Donohoe, TS L’Ecuyer, Constraining atmospheric heat transport from earth energy budget observations. *J. Clim.* **38**, 5129–5144 (2025).
44. FR Robertson, et al., Uncertainties in ocean latent heat flux variations over recent decades in satellite-based estimates and reduced observation reanalyses. *J. Clim.* **33**, 8415–8437 (2020).
45. KE Trenberth, Climate diagnostics from global analyses: Conservation of mass in ecmwf analyses. *J. Clim.* **4**, 707–722 (1991).
46. T Cox, A Donohoe, KC Armour, GH Roe, DM Frierson, A new method for calculating instantaneous atmospheric heat transport. *J. Clim.* **37**, 4337–4346 (2024).
47. M Sprenger, H Wernli, The lagranto lagrangian analysis tool–version 2.0. *Geosci. Model. Dev.* **8**, 2569–2586 (2015).
48. A Said, WA Pearlman, A new, fast, and efficient image codec based on set partitioning in hierarchical trees. *IEEE Transactions on circuits systems for video technology* **6**, 243–250 (1996).
49. R Puchinger, ImShrinker - SPIHT algorithm implementation (<https://github.com/gilson27/imshrinker>) (2017) Last modified in 2017. Originally created in 2008, revised in 2013. A minimal console implementation of the SPIHT algorithm from the paper by A. Said and W. A. Pearlman (1996).
50. CS Zender, Analysis of self-describing gridded geoscience data with netcdf operators (ncio). *Environ. Model. & Softw.* **23**, 1338–1342 (2008).
51. U Schulzweida, Cdo user guide (2023).
52. S Hoyer, J Hamman, xarray: N-D labeled arrays and datasets in Python. *J. Open Res. Softw.* **5** (2017).
53. T Vincent, et al., siix-kit/hdf5plugin: 5.1.0: 31/03/2025 (2025).

# PNAS



## Supporting Information for

### Error bounded compression for weather and climate applications

Langwen Huang, Luigi Fusco, Florian Scheidl, Jan Zibell, Michael Armand Sprenger, Sebastian Schemm, and Torsten Hoefler

Langwen Huang

E-mail: langwen.huang@inf.ethz.ch

#### This PDF file includes:

Figs. S1 to S10

Table S1

DRAFT

## Definitions of Error Metrics

Denote  $A$  as the original data chunk,  $A'$  as the reconstructed chunk after lossy compression and decompression, and  $n$  as the number of elements in  $A$ . The definitions of error metrics are as follows.

**Table S1. Error metrics and their mathematical definitions.**

Metric	Formula
Maximum absolute error	$\max_{\forall i \in [1, n]}  A'_i - A_i $
Range-relative maximum absolute error	$\frac{\max_{\forall i \in [1, n]}  A'_i - A_i }{\max_{\forall i \in [1, n]} A_i - \min_{\forall i \in [1, n]} A_i}$
Root mean square error (RMSE)	$\sqrt{\frac{\sum_{i=1}^n (A'_i - A_i)^2}{n}}$

## Histograms

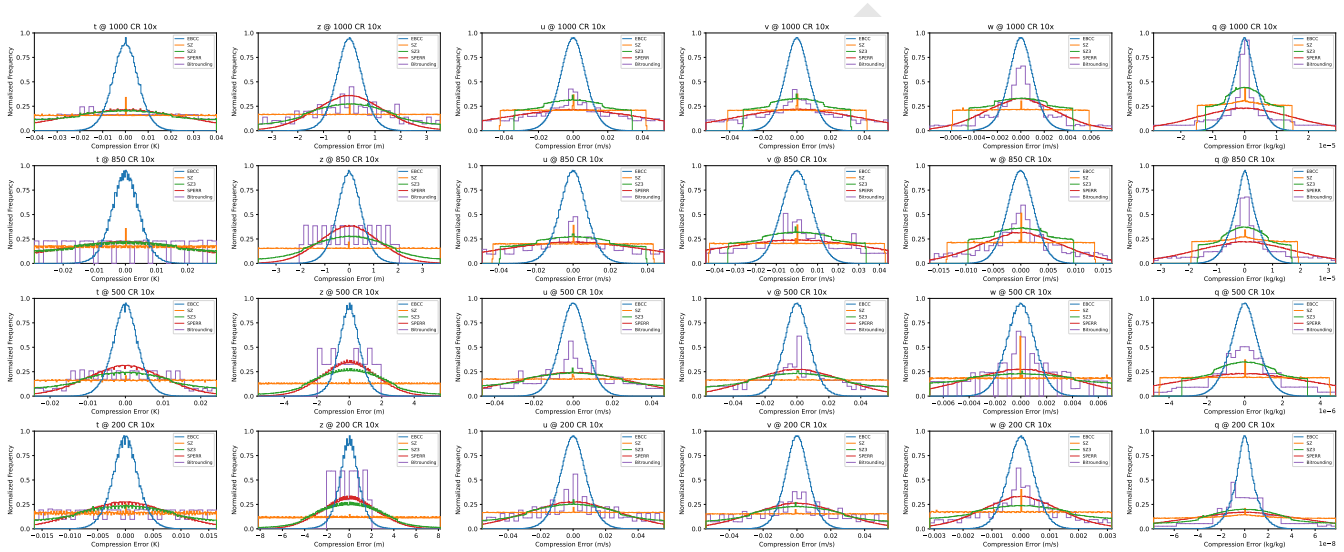


**Fig. S1. Histograms of compression errors for pressure-level variables at a compression ratio of 10x.**

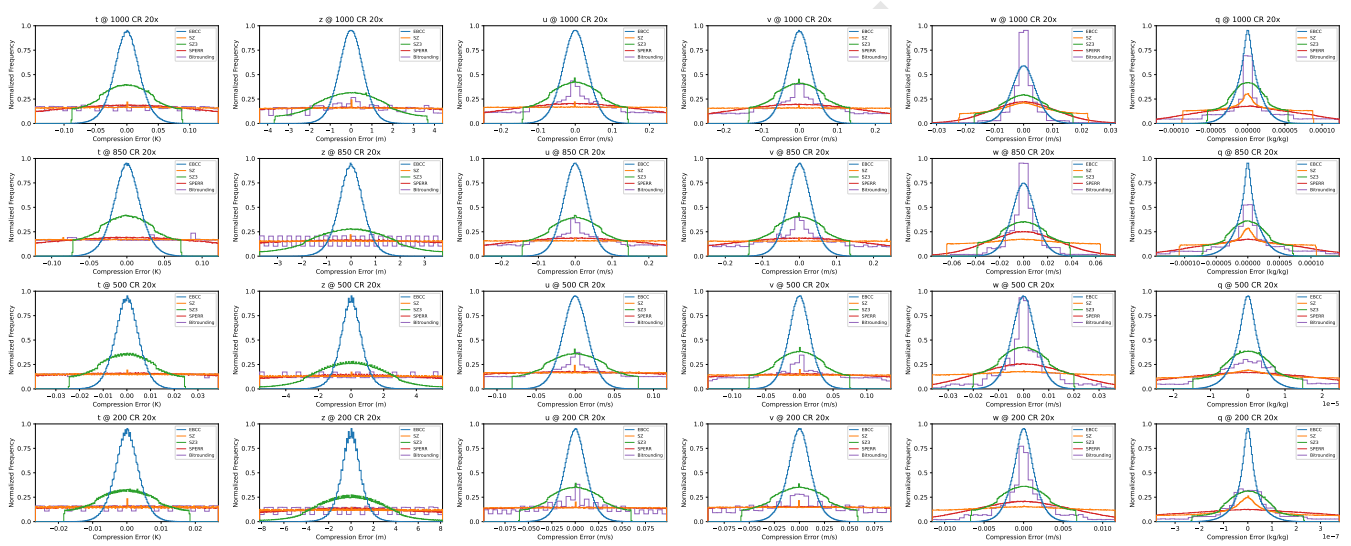


Fig. S2. Histograms of compression errors for pressure-level variables at a compression ratio of 20x.

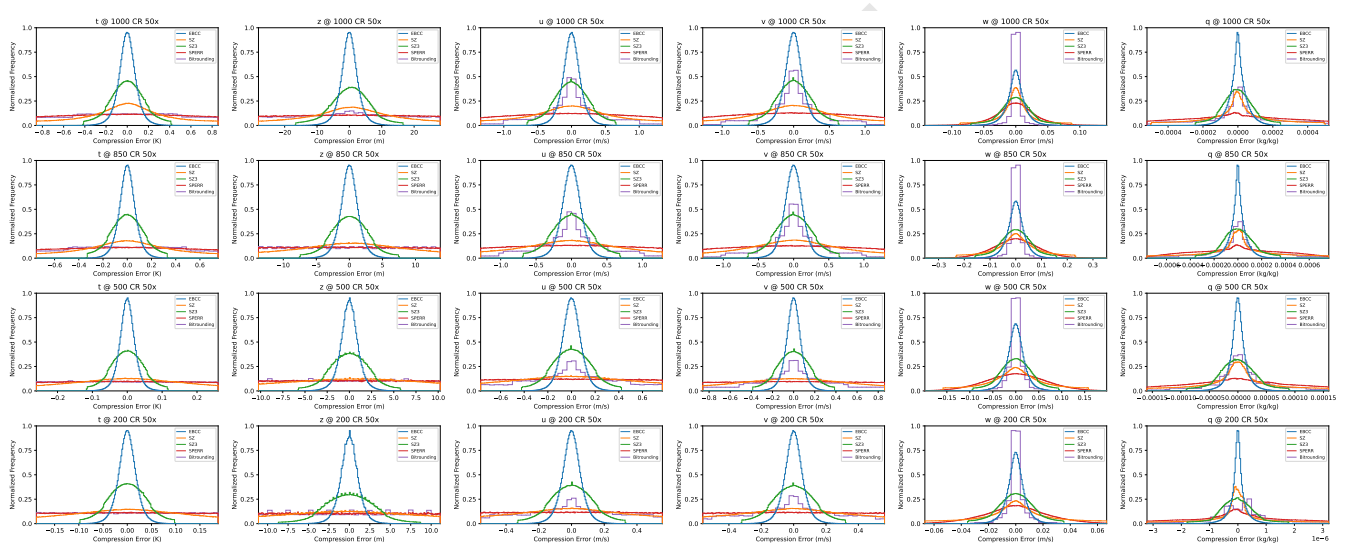


Fig. S3. Histograms of compression errors for pressure-level variables at a compression ratio of 50x.

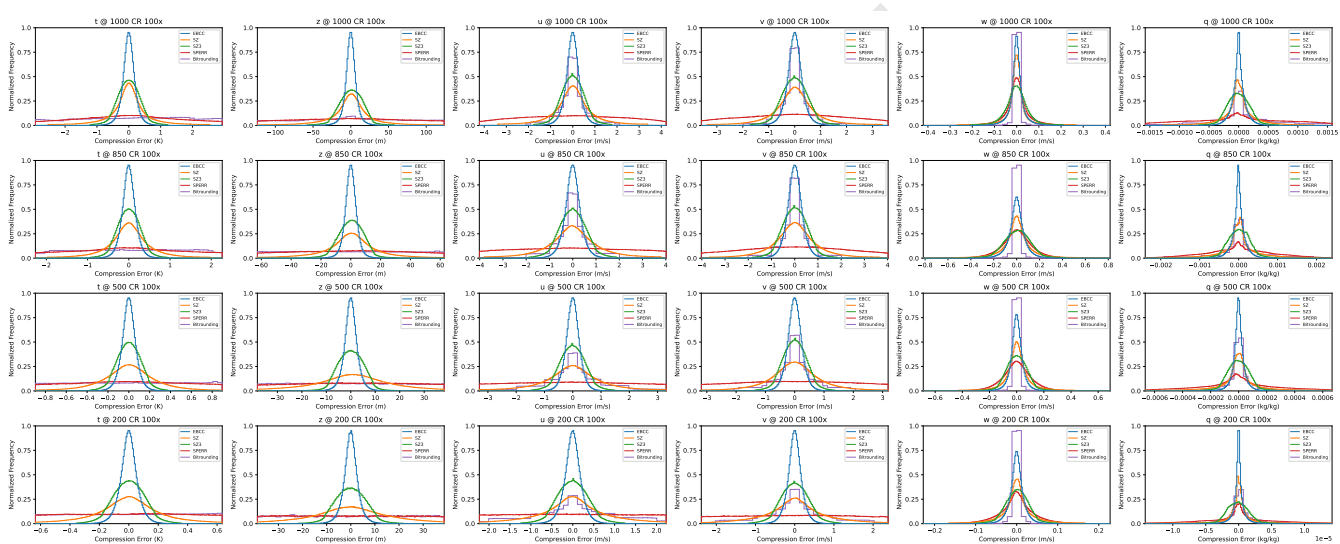


Fig. S4. Histograms of compression errors for pressure-level variables at a compression ratio of  $100\times$ .

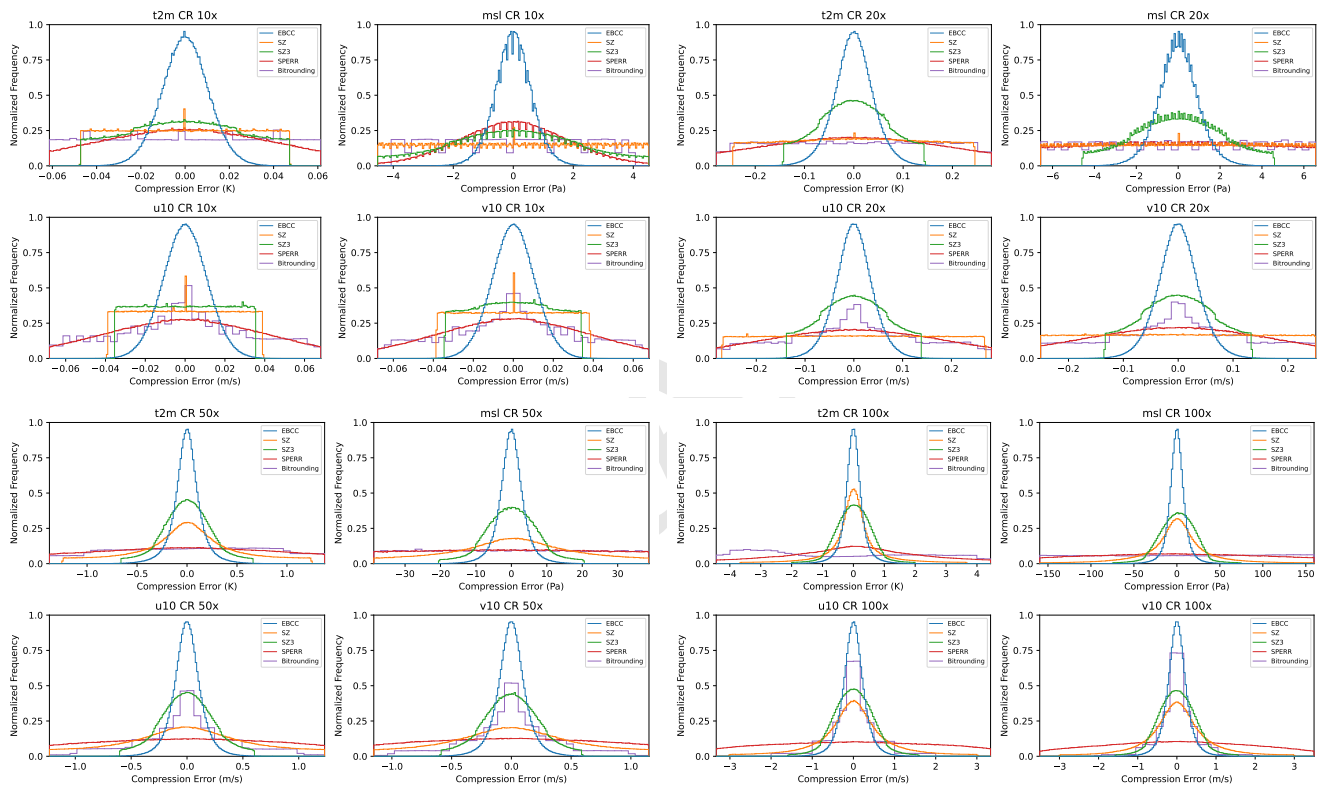


Fig. S5. Histograms of compression errors for surface variables at compression ratios of 10 $\times$ , 20 $\times$ , 50 $\times$ , and 100 $\times$ .

# Power Spectra

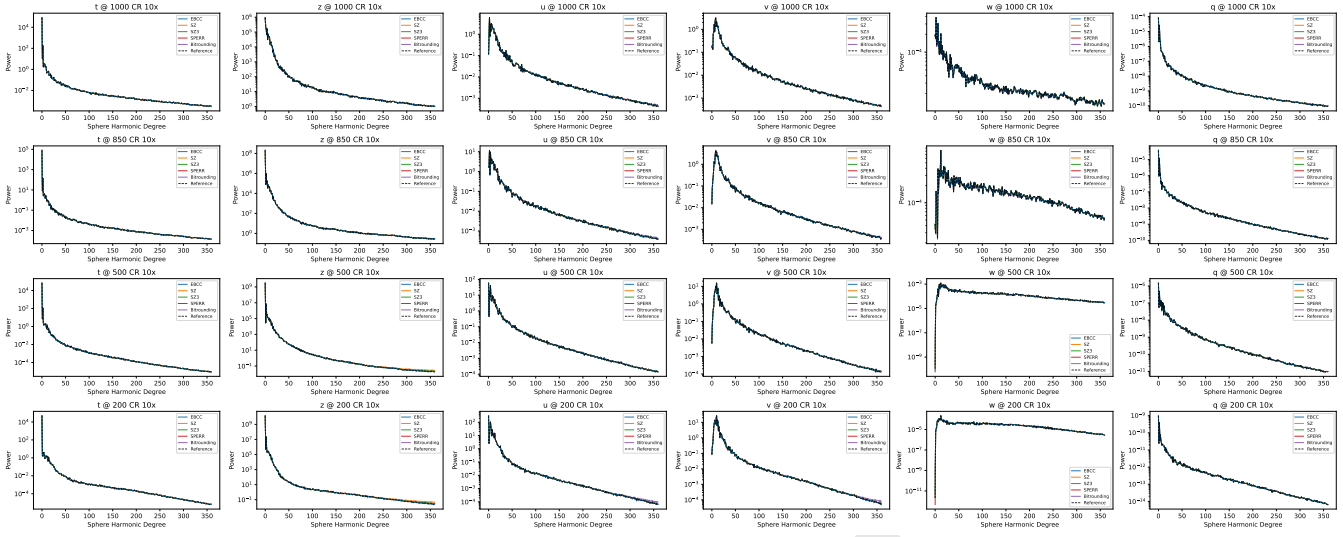


Fig. S6. Spherical harmonics power spectra of compression errors for pressure-level variables at a compression ratio of 10x.

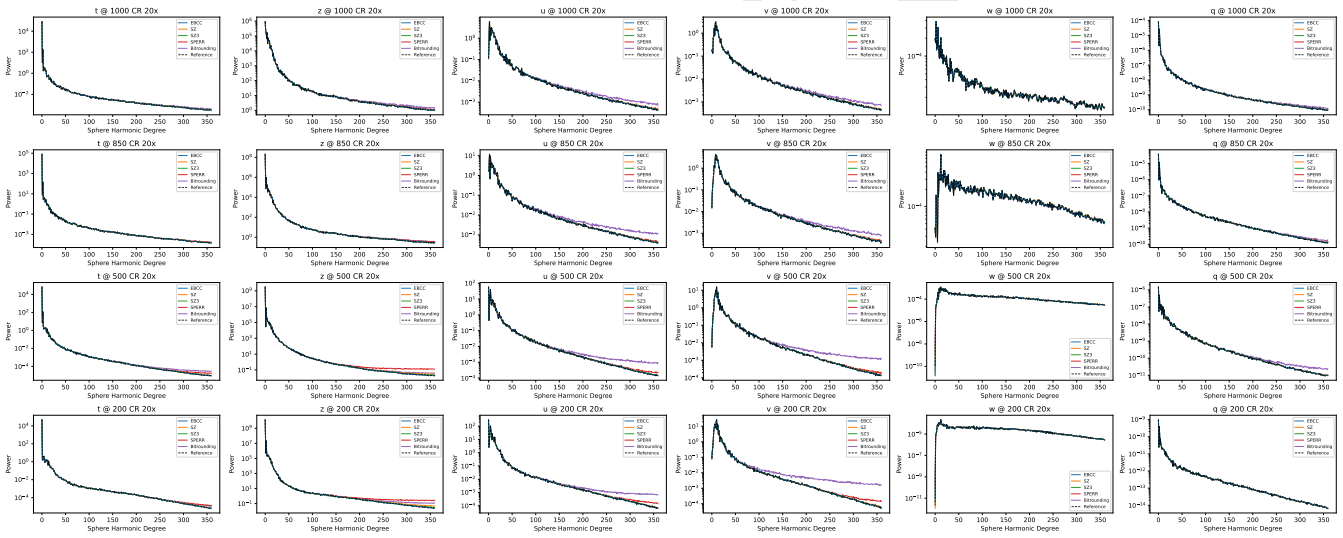


Fig. S7. Spherical harmonics power spectra of compression errors for pressure-level variables at a compression ratio of 20x.



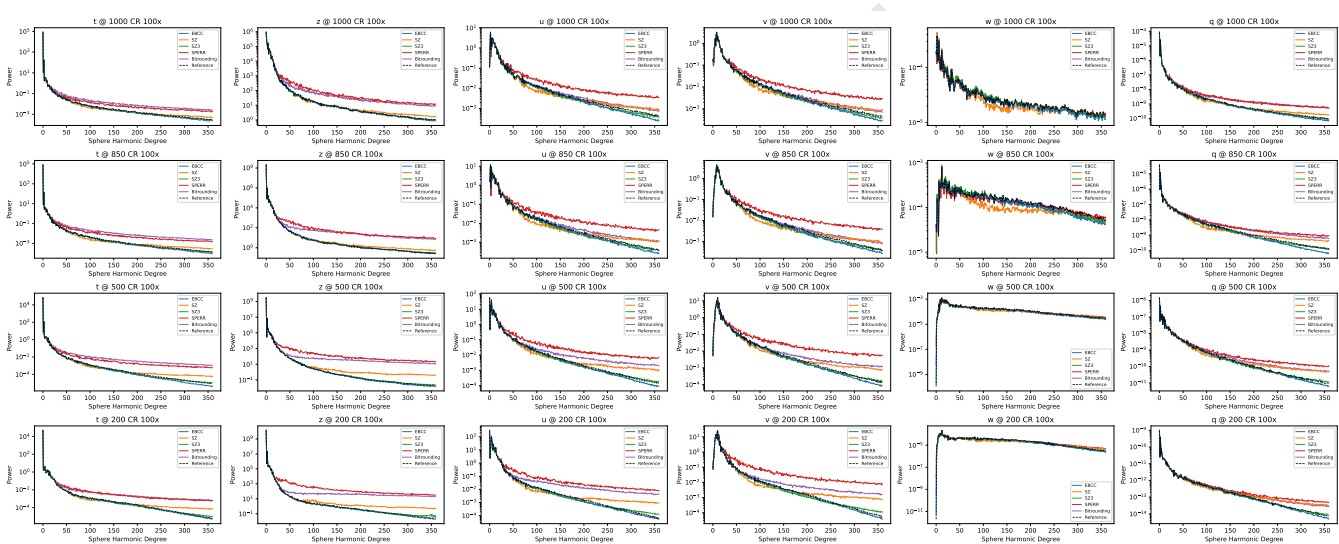


Fig. S9. Spherical harmonics power spectra of compression errors for pressure-level variables at a compression ratio of 100x.

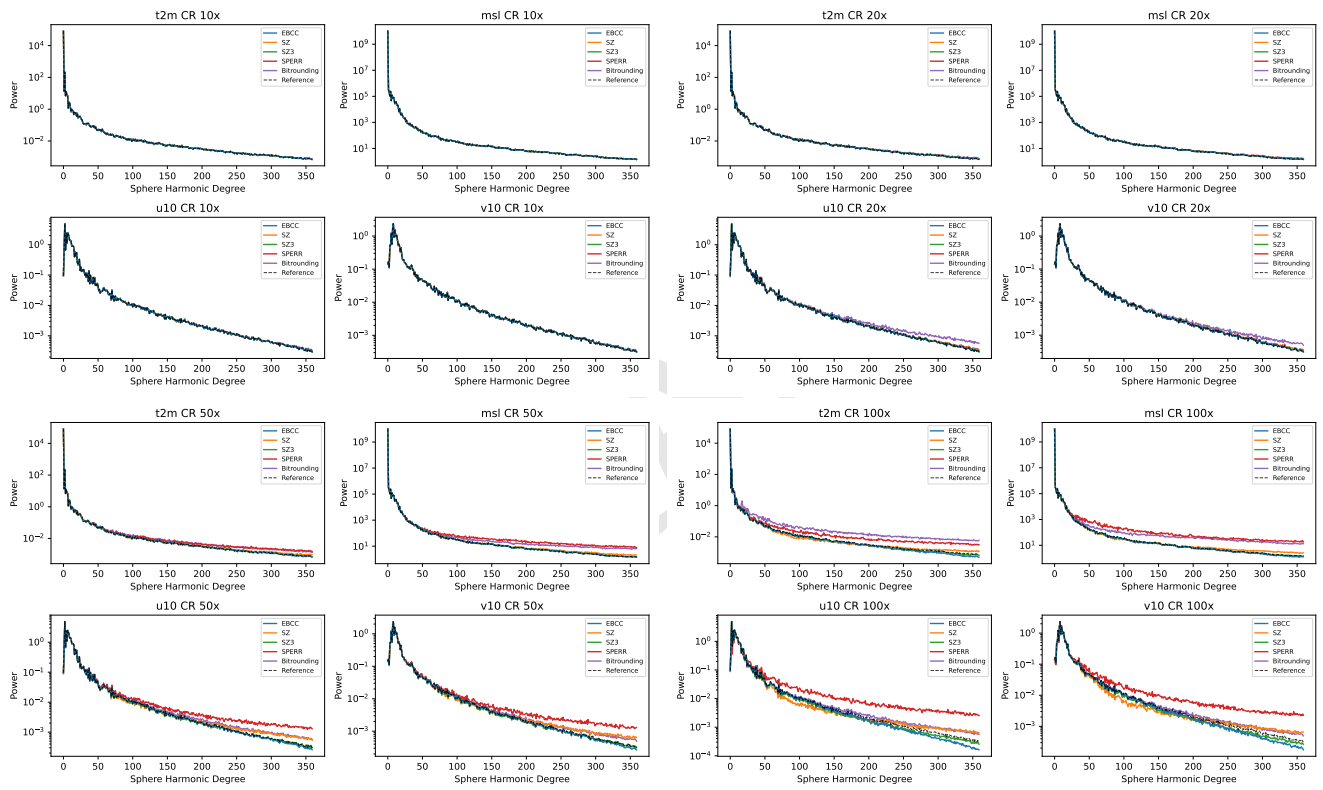


Fig. S10. Spherical harmonics power spectra of compression errors for surface variables at compression ratios of 10 $\times$ , 20 $\times$ , 50 $\times$ , and 100 $\times$ .